Shear stress tensor and specific shear viscosity of hot hadron gas in nuclear collisions

Zhidong Yang* and Rainer J. Fries†

Cyclotron Institute and Department of Physics and Astronomy, Texas A&M University, College Station, Texas 77843, USA

(Received 18 October 2021; accepted 29 November 2021; published 14 January 2022)

We extract the shear stress tensor of nuclear matter in the hadronic phase in high energy nuclear collisions. We use a blast-wave parametrization of the final state of nuclear collisions, including nonequilibrium deformations of particle distributions due to shear stress in the Navier-Stokes approximation. We fit spectra and elliptic flow of identified hadrons for a variety of collision energies and impact parameters at the Relativistic Heavy Ion Collider (RHIC) and the Large Hadron Collider (LHC). The systems analyzed cover a temperature range from about 110 to 150 MeV and vary in their chemical potentials for stable hadrons. We then attempt to estimate the specific shear viscosity η/s of nuclear matter for various temperatures and chemical potentials in the hadronic phase. We assign systematic uncertainties to our results. Using a recent systematic study of fluid dynamics pseudodata with the same blast-wave model [Z. Yang and R. J. Fries, arXiv:2007.11777], we apply a correction to the raw fit results which removes some biases typical for blast-wave fits. This work is complementary to efforts using viscous fluid dynamics to extract the specific shear viscosity of quark gluon plasma at higher temperatures. We put our work in context with existing theoretical calculations of the specific shear viscosity.

DOI: 10.1103/PhysRevC.105.014910

I. INTRODUCTION

Quark gluon plasma (QGP) and hot hadron gas are routinely created in nuclear collisions at the Relativistic Heavy Ion Collider (RHIC) and the Large Hadron Collider (LHC). Soon after the start of the RHIC program it was realized that experimental data from this machine required a new paradigm. Although the original motivation for postulating the existence of quark gluon plasma came from the known weakening of the strong coupling constant with temperature [1,2], it turned out that QGP close to the pseudocritical temperature T_c, i.e., at temperatures probed by the experimental programs at RHIC and LHC, rather behaves like a strongly coupled liquid [3,4]. The first hint came from the great success enjoyed by *ideal* fluid dynamics in describing the flow of hadrons measured at RHIC [5,6]. As it turns out, the process of cooling and expansion of the fireball of QGP and hadron gas behaves hydrodynamically from very early times in the collision onward. Subsequently, relativistic *viscous* fluid dynamic simulations compared to data allowed the quantitative extraction of η/s from data [7–10]. Around the same time, Kovtun, Son, and Starinets hypothesized that there might be a universal lower bound of $\eta/s = 1/(4\pi)$ for the specific shear viscosity, based on their study of strongly interacting systems using anti–de Sitter and conformal field theory (AdS/CFT) correspondence [11]. Quark gluon plasma quickly became a celebrated example of an ideal liquid.

Measurements of the specific shear viscosity η/s utilize viscous fluid dynamic simulations compared to experimental data. Collective flow observables are particularly sensitive to shear viscosity. The first generation of calculations used relativistic fluid dynamics with a fixed, temperature-independent η/s as a parameter. Fluid dynamics was run all the way to kinetic freeze-out in the hadronic phase, which was modeled very similarly to the approach discussed further below here. Obviously the value of η/s extracted from this method is averaged over the entire temperature evolution of the QGP *and* the hot hadron gas below T_c, a range of several hundred MeV at top RHIC and LHC energies. η/s extracted through this method also includes the effects of deformations of particle distributions at freeze-out that are present at finite shear stress [8,12].

Subsequently, several groups argued that the hadronic phase should be rather described by hadronic transport models because the specific shear viscosity in the hadronic phase could be too large for the evolution to be described accurately in second-order viscous fluid dynamic codes [13,14]. This argument was aided by estimates of η/s for hadron gas from chiral perturbation theory, effective theories, and hadronic transport by various groups [15–25]. While these calculations do not agree quantitatively, they often find rather large specific shear viscosity for a hot hadron gas, $\eta/s \gtrsim 4/(4\pi)$ even very close to T_c, in particular the calculations based on the URQMD and SMASH transport models; see Fig. 8. Thus fluid dynamic calculations are typically matched to hadronic transport models just below T_c while η/s is retained as a parameter only for the QGP phase and the crossover region around T_c. Even more recently, fluid dynamic calculations using simple parametrizations have also been used to constrain the functional form of the temperature dependence of η/s, mostly for the QGP case [13,26,27]. We refer the reader to [10,28,29] for reviews of fluid dynamic simulations of nuclear collisions, including the extraction of shear viscosity.

*zdyang07@163.com
†rjfries@comp.tamu.edu

Lattice calculations of η/s in the QGP phase have been attempted but are challenging [30–34]. They generally find η/s to be close to the conjectured lower bound around T_c with a rather slow rise towards higher temperatures. Perturbative QCD calculations at leading order have indicated large values of η/s at temperatures well above T_c [35,36], but a recent next-to-leading order calculation predicts a significant drop towards T_c which makes the perturbative results comparable to lattice QCD [37].

From general arguments one expects a minimum of η/s around T_c, which has been found to be the case for a large variety of systems [38]. How fast the specific shear viscosity is rising towards lower temperatures below T_c cannot be seen as settled from either data or first-principle calculations. Features should be continuous as a function of temperature but could be changing quickly. Progress has been made in understanding the large values of η/s in hadronic transport [24]. However, these effective theories mostly do not incorporate the existence of a pseudocritical temperature, and their predictions close to this temperature should be viewed with caution. The question of the specific shear viscosity of hadron gas is an important one. In any conceivable experiment information on specific shear viscosity in the QGP phase is always convoluted with contributions from the hadronic phase. Thus uncertainties in hadronic η/s are directly responsible for increased uncertainties of QGP shear viscosities extracted from data.

It is clear that an independent assessment of the hadronic specific shear viscosity is necessary to improve the situation. As a reasonable minimum requirement, theoretical uncertainties coming from incomplete knowledge of the hadronic phase should inform realistic contributions to error bars for quantities extracted for the QGP phase. For this reason we attempt to estimate uncertainties in this work. Moreover, the specific shear viscosity of a hot hadron gas is by itself a compelling question.

In this work we extract the shear stress of hot hadronic matter in high energy nuclear collisions from experimental data. We will further argue that it is possible to use experimental data to estimate the specific shear viscosity of the hot hadron gas at the kinetic freeze-out. The main effect of the time evolution of the system before freeze-out is the buildup of a flow field u^μ which leads to the system expanding and cooling. Viscous corrections to first order are given by gradients of the flow field (Navier-Stokes approximation). Computing the flow field in fluid dynamics introduces additional dependences on initial conditions and the equation of state. We take a complementary approach and *fit* the final flow field, together with the temperature and system size at kinetic freeze-out. The shear stress tensor in the Navier-Stokes approximation can then be assumed to be proportional to the symmetric and traceless gradient tensor of the flow field. The viscosity is the proportionality constant in this approximation. The resulting specific shear viscosity is a parameter at just one fixed temperature $T = T_{\rm fo}$, the kinetic freeze-out temperature, and a set of chemical potentials $\mu_{\rm fo} = (\mu_B, \mu_\pi, \ldots)$ for baryon number B, and abundances of stable hadrons like pions, kaons, and nucleons. Of course, such fits of flow fields and temperatures at freeze-out are well established and generally known as blast-wave parametrizations [39–41]. We will use such a blast wave, with η/s added as a parameter, to extract $\eta/s(T_{\rm fo}, \mu_{\rm fo})$ for a variety of points $(T_{\rm fo}, \mu_{\rm fo})$ in different collision systems. Here we present the results for Au + Au collisions at top RHIC energies and Pb + Pb collisions at LHC where the baryon chemical potential vanishes, $\mu_B \approx 0$. However, nonvanishing chemical potentials μ_π, μ_K, and μ_p are present at kinetic freeze-out, determined by the chemical freeze-out at higher temperatures. Our extraction is complementary to fluid dynamics, which integrates over the effects of shear viscosity over a wide temperature range. Some of the uncertainties in both approaches are the same. For example the assumption of a sharp kinetic freeze-out at a fixed temperature is common to both approaches and is only an approximation, although it can be improved in the case of fluid dynamics by matching to hadronic transport. Other uncertainties are different in both approaches. For example the dependence of fluid dynamic calculations on initial conditions, which themselves are not well constrained experimentally, is not present in our approach. We will discuss uncertainties in the blast-wave extraction in more detail below. We also attempt to remove the systematic bias that the simplicity of the blast-wave ansatz introduces when compared to full fluid dynamic calculations. This paper is organized as follows: In Sec. II we present our blast-wave parametrization, especially the viscous correction term. In Sec. III we discuss the simulation and data selection. In Sec. IV we show fit results and carry out an analysis of uncertainties. We conclude with a discussion and outlook in Sec. V.

II. A VISCOUS BLAST WAVE

Viscous corrections to blast waves have been studied in [12,42]. Both of these previous works assume spatial spherical symmetry in the transverse plane and free streaming for simplicity. We will generalize these assumptions here. We choose the blast wave of Retiere and Lisa (RL) [41] as our starting point. In this section we discuss the Retiere-Lisa blast wave and compute the Navier-Stokes corrections.

We have to make two major assumptions in our analysis, both of which have been routinely used and studied in the literature. The first is that at freeze-out the system of hadrons is close enough to kinetic equilibrium so that at any position $r^\mu = (t, x, y, z)$ there exist a local rest frame with a local temperature $T_{\rm fo}(r)$ and a set of chemical potentials $\mu_{\rm fo}(r)$ such that the particle distribution in the local rest frame can be written as

$$f(r, p) = f_0(r, p) + \delta f(r, p), \tag{1}$$

where f_0 is the equilibrium Bose/Fermi distribution with the local temperature and chemical potentials,

$$f_0(r, p) = \frac{1}{e^{[E-\mu(r,p)]/T_{\rm fo}(r,p)} \mp 1}, \tag{2}$$

and δf is the correction due to nonvanishing gradients. Here we use the general form

$$\delta f(r, p) = \frac{1}{2s}\frac{\Gamma(6)}{\Gamma(4+\lambda)}\left(\frac{E}{T_{\rm fo}}\right)^{\lambda-2}\frac{p_\mu p_\nu}{T_{\rm fo}^3}\pi^{\mu\nu} f_0(r, p) \tag{3}$$

which follows from a generalized Grad ansatz [43]. $\pi^{\mu\nu}$ is the shear stress tensor. In the Navier-Stokes approximation it can be expressed as $\pi^{\mu\nu} = 2\eta\sigma^{\mu\nu}$, where the traceless shear gradient tensor is defined as

$$\sigma^{\mu\nu} = \tfrac{1}{2}(\nabla^\mu u^\nu + \nabla^\nu u^\mu) - \tfrac{1}{3}\Delta^{\mu\nu}\nabla_\lambda u^\lambda. \tag{4}$$

Here $\nabla^\mu = \Delta^{\mu\nu}\partial_\nu$, with $\Delta^{\mu\nu} = g^{\mu\nu} - u^\mu u^\nu$, is the derivative perpendicular to the flow field vector u^μ. The gradient corrections need to be small and we will ensure that numerically $\delta f \lesssim f$ for all relevant momenta in this analysis. The power λ in Eq. (3) parametrizes further details of the underlying microscopic physics. We restrict ourselves to the original Grad ansatz $\lambda = 2$ which is widely used. We reserve a more detailed analysis including λ as a tunable parameter for future work.

The second major assumption in our analysis pertains to the simplified shape of the freeze-out hypersurface and flow field. In longitudinal direction (along the colliding beams) we assume boost invariance, which is a good approximation for particles measured around midrapidity at LHC and top RHIC energies. Blast wave parametrizations assume that freeze-out happens at constant $T_{\rm fo}$ and $\mu_{\rm fo}$, which is approximated by a constant (longitudinal) proper time $\tau = \tau_{\rm fo}$. In the RL parametrization the transverse shape of the fireball at freeze-out is assumed to be an ellipse with semiaxes R_x and R_y in x and y directions respectively. We define the coordinate axes such that the impact parameter b of the collision is measured along the x axis. In the following we use the reduced radius $\rho = \sqrt{x^2/R_x^2 + y^2/R_y^2}$. The flow field can be parametrized as

$$u^\mu = (\cosh\eta_s \cosh\eta_T, \sinh\eta_T \cos\phi_u, \sinh\eta_T \times \sin\phi_u, \sinh\eta_s \cosh\eta_T), \tag{5}$$

where η_T is the transverse rapidity in the x-y plane and ϕ_u is the azimuthal angle of the flow vector in the transverse plane. Boost invariance fixes the longitudinal flow rapidity to be equal to the space-time rapidity $\eta_s = \ln[(t+z)/(t-z)]/2$. For the transverse flow velocity $v_T = \tanh\eta_T$ we make the assumption [41]

$$v_T = \rho^n[\alpha_0 + \alpha_2\cos(2\phi_u)], \tag{6}$$

which encodes a Hubble-like velocity ordering with an additional shape parameter n. α_0 is the average velocity on the boundary $\rho = 1$, and α_2 parameterizes an elliptic deformation of the flow field coming from the original elliptic spatial deformation of systems with finite impact parameters. The time evolution of pressure gradients in the expansion leads to flow vectors tilted towards the smaller axis of the ellipse. This is accomplished by demanding that the transverse flow vector is perpendicular to the elliptic surface at $\rho = 1$, i.e., $\tan\phi_u = (R_x^2/R_y^2)\tan\phi$, where $\phi = \arctan y/x$ is the azimuthal angle of the position r^μ. Higher order deformations could be present [42], but the two main observables chosen for our analysis are not particularly sensitive to them. We want to emphasize that the simplifications of a blast wave compared to fluid dynamics can be studied systematically. We have done so in an accompanying work [44]. Further below we will use the results from this comparison to correct systematic biases introduced by the simplistic freeze-out hypersurface and flow field.

Using the assumptions laid out here we can write the spectrum of hadrons emitted from freeze-out as [45]

$$\frac{dN}{dy\,d^2P_T} = g\int \frac{p\cdot d\Sigma}{(2\pi)^3} f(r, u\cdot p), \tag{7}$$

where g is the degeneracy factor for a given hadron. The momentum vector in the laboratory frame is written in standard form as $p^\mu = (M_T\cosh y, P_T\cos\psi,\ P_T\sin\psi, M_T\sinh y)$ in terms of the transverse momentum P_T, the longitudinal momentum rapidity y, and the azimuthal angle ψ in the transverse plane. $M_T^2 = P_T^2 + M^2$ defines the transverse mass M_T for a hadron of mass M. $d\Sigma^\mu$ is a parametrization of the $T = T_{\rm fo}$ hypersurface and its outbound normal vector. With our assumptions we have $d\Sigma^\mu = \tau_{\rm fo}R_xR_y d\eta_s\rho\, d\rho\, d\theta(\cosh\eta_s, 0, 0, \sinh\eta_s)$. Hence, for hadrons measured around midrapidity ($y = 0$) the spectrum takes the standard form

$$\frac{dN}{dy\,d^2P_T} = g\tau_{\rm fo}R_xR_yM_T\int_0^1 d\rho\int_0^{2\pi} d\theta\int_{-\infty}^{\infty} d\eta_s \frac{\rho\cosh\eta_s}{(2\pi)^3} \times f_0(\rho,\theta,\eta_s; u\cdot p)\left[1 + \frac{\eta}{s}\frac{1}{T_{\rm fo}^3}p_\mu p_\nu\sigma^{\mu\nu}\right], \tag{8}$$

where $\tan\theta = (R_x/R_y)\tan\phi$. The set of parameters in this ansatz is $\tilde{\mathcal{P}} = (\tau_{\rm fo}, R_x, R_y, T_{\rm fo}, \mu_{\rm fo}, n, \alpha_0, \alpha_2, \eta/s)$.

We can now determine the shear gradient tensor $\sigma^{\mu\nu}$ for the RL blast wave, following the example of [12,42]. Without azimuthal symmetry the spatial derivatives in $\sigma^{\mu\nu}$ are still straightforward to obtain, starting from the explicit expression in Eq. (5), but the results are somewhat lengthy. We delegate a discussion of details of these expressions to another work. The task of determining the time derivatives in $\sigma^{\mu\nu}$ can be reduced to the question of computing $\partial_\tau\eta_T$ and $\partial_\tau\phi_u$. We start from the relativistic fluid dynamic equations of motion $\partial_\mu T^{\mu\nu} = 0$, where $T^{\mu\nu} = eu^\mu u^\nu - p\Delta^{\mu\nu}$ is the ideal energy momentum tensor. We can restrict ourselves to ideal fluid dynamics to obtain the leading order expressions in a gradient expansion for the time derivatives. Dissipative corrections in the determination of the time derivatives would lead to terms of order $\eta^2 \times$ (second-order spatial gradients) in δf which we neglect. Here e is the local energy density and p the pressure. The ideal fluid dynamics equations can be rewritten more instructively as the set of equations

$$De = -(e+p)\partial_\mu u^\mu = -(e+p)\nabla_\mu u^\mu, \tag{9}$$

$$Du^\mu = \frac{\nabla^\mu p}{e+p}, \tag{10}$$

where the comoving time derivative is $D = u_\mu\partial^\mu$.

Freeze-out is the process of decoupling of particles where the mean free path rapidly grows beyond the system size. In fluid dynamics this process is modeled through a sudden transition during which the mean free path goes from very small values to infinity instantaneously at $T = T_{\rm fo}$. The system is free streaming, $Du^\mu = 0$, after the transition, i.e., from $T = T_{\rm fo} - \epsilon$ on (with small $\epsilon > 0$). Thus the assumption of free streaming has been used in some previous work on viscous blast waves [12,42]. However, it seems more physical to assume that the local particle distributions $f(r, p)$ remain frozen

across the $T = T_{\rm fo}$ hypersurface and that $\sigma^{\mu\nu}$, including time derivatives, should be set at temperature $T = T_{\rm fo} + \epsilon$. This is consistent with the treatment in fluid dynamics. Equations (9) and (10) can be solved for the blast-wave geometry and flow field assumed here to obtain the time derivatives we seek.

Using (9) together with the first or fourth equation ($\mu = 0, 3$; the two equations are equivalent) in (10) we obtain the time derivative of the transverse flow rapidity,

$$\begin{aligned}(1 - c_s^2 \tanh^2 \eta_T)\partial_\tau \cosh \eta_T \\ = c_s^2 \tanh^2 \eta_T \left(\partial_1 u^1 + \partial_2 u^2 + \frac{\cosh \eta_T}{\tau} \right) \\ - \frac{u^1 \partial_1 u^0}{u^0} - \frac{u^2 \partial_2 u^0}{u^0},\end{aligned} \tag{11}$$

in terms of known spatial derivatives. $c_s^2 = \partial p / \partial e$ is the speed of sound squared, given by the equation of state of the system at $T = T_{\rm fo}$. The time derivative of the direction of the transverse flow field can be computed by using (11) in the second and third equations ($\mu = 1, 2$) in (10).

It will be useful to analyze the shear stress tensor $\pi^{\mu\nu}$ as a quantity which relies somewhat less on the applicability of the Navier-Stokes approximation. In this work we will therefore analyze the dimensionless ratio $\pi^{\mu\nu}/(e + p)$, where e and p are the equilibrium energy density and pressure. This particular quantity can be easily computed from parameters extracted from the fit procedure as

$$\frac{\pi^{\mu\nu}}{e + p} = \frac{2}{T_{\rm fo}} \frac{\eta}{s} \sigma^{\mu\nu}, \tag{12}$$

and it can be easily converted into other dimensionless ratios of shear stress with equilibrium quantities using the equation of state.

This completes the brief introduction of the blast-wave model used in our analysis. One can validate the blast wave by comparison with established fluid dynamics calculations. We have done so in Ref. [44] using the viscous fluid code MUSIC [46,47]. The implications of the results of Ref. [44] for this work are discussed in detail below.

III. SIMULATION AND DATA SELECTION

With $\sigma^{\mu\nu}$ known it is straightforward to evaluate Eq. (8) numerically, dependent on the set of parameters $\tilde{\mathcal{P}}$ which can be determined from the fits to data or other methods. We carry out this analysis using data on identified protons and antiprotons, kaons, and pions from LHC and RHIC. We utilize both transverse momentum spectra around midrapidity and elliptic flow v_2, the leading harmonic deformation of the spectrum in azimuthal momentum space angle ψ, as functions of hadron transverse momentum P_T. They are calculated from (8) as

$$\frac{dN}{2\pi P_T dP_T dy} = \frac{1}{2\pi} \int d\psi \frac{dN}{dy\, d^2P_T}, \tag{13}$$

$$v_2(P_T) = \left(\frac{dN}{2\pi P_T dP_T dy} \right)^{-1} \frac{1}{2\pi} \int d\psi \cos(2\psi) \frac{dN}{dy\, d^2P_T}, \tag{14}$$

respectively. Note that the blast wave does not incorporate fluctuations. This is one reason why we will not analyze the most central and peripheral centrality bins available, which are known to exhibit large effects due to fluctuations. All expressions in the blast wave are taken at rapidity $y = 0$ and we have utilized matching data sets that have been taken around midrapidity.

We use data from the ALICE Collaboration for Pb + Pb collisions at 2.76 TeV [48,49], in 10% centrality bins, and from the PHENIX Collaboration for Au + Au collisions at 200 GeV [50,51]. The PHENIX data are binned in 10% or 20% centrality bins for the spectra and 10% centrality bins for elliptic flow. For this analysis, if the PHENIX spectrum is only available in a coarser bin we combine a given 10% bin for elliptic flow together with the overlapping 20% bin for the spectrum. We find that centralities that share the coarser spectrum bins give results for temperature and specific shear viscosity that agree very well with each other within estimated uncertainties.

The selection of data points for the fit can introduce a bias that we try to quantify as an uncertainty. The following general principles were applied in the selection. We expect the blast-wave parametrization to extract inaccurate parameters at too low momenta where resonance decays dominate the spectrum [52]. We also expect it to fail at too large momentum where gradient corrections become large, and hadrons from other production channels, like hard processes, start to dominate soft particles from the bulk of the fireball. The maximum momentum P_T described by the blast wave increases from peripheral to more central collisions, since particles are expected to be more thermalized when volumes and lifetimes are larger. In addition, flow pushes particles with the same velocity to higher momentum if their mass is larger. Thus fit ranges for heavier particles can extend farther.

Using these guiding principles we choose a preferred fit range in transverse momentum for each centrality, collision energy, and particle species. We call this selection the regular fit range (RFR). For example, the regular fit range for the ALICE data in the 30–40% centrality bin uses data points for the spectra in the P_T intervals 0.325–3.10, 0.225–2.25, and 0.525–1.65 GeV/c for protons, kaons, and pions, respectively. The RFR for all data sets used here is shown in Table I. The v_2 data points included in this analysis are chosen to be consistent with the spectrum data points. We note that our fit ranges for ALICE data extend to higher momentum compared to the fit ranges previously used by the ALICE Collaboration for their blast-wave fits without viscous corrections [53]. For each data set we supplement the regular fit ranges with lower (LFR) and higher (HFR) fit ranges in an attempt to quantify uncertainties from fit range selection. This will be discussed in detail in the next section.

We use the statistical analysis package from the Models and Data Analysis Initiative (MADAI) project [54,55] to determine fit parameters. The MADAI package includes a Gaussian process emulator and a Bayesian analysis tool. A single computation of Eq. (8) is quite fast. The Gaussian process emulator allows us to carry out the full statistical analysis easily on a single CPU. We choose appropriate prior ranges for each parameter (see Fig. 1 for an example) with flat prob-

TABLE I. Regular fit range (RFR) selected for each ALICE and PHENIX centrality bin for the spectra of all three particle species. The bins for elliptic flow data are chosen consistently. We also show the average impact parameter b from Glauber Monte Carlo calculations quoted by the experiments, the speed of sound squared c_s^2, and the expansion parameter c_τ determined for each data set. For PHENIX data the average impact parameter for the two 10% bins included in a given 20% bin are quoted in parentheses.

Centrality	Proton (GeV/c)	Kaon (GeV/c)	Pion (GeV/c)	b (fm)	c_s^2	c_τ
			ALICE 2.76 TeV			
10–20%	0.325–3.3	0.225–2.55	0.525–1.85	6.05	0.158	0.783
20–30%	0.325–3.1	0.225–2.35	0.525–1.75	7.81	0.162	0.756
30–40%	0.325–3.1	0.225–2.25	0.525–1.65	9.23	0.166	0.720
40–50%	0.325–2.95	0.225–2.15	0.525–1.45	10.47	0.170	0.679
50–60%	0.325–2.55	0.225–1.85	0.525–1.25	11.58	0.174	0.633
			PHENIX 0.2 TeV			
10–20%	0.55–2.9	0.55–1.85	0.55–1.65	5.70	0.164	0.780
20–40%	0.55–2.7	0.55–1.75	0.55–1.55	8.10 (7.4, 8.7)	0.170	0.739
40–60%	0.55–2.5	0.55–1.65	0.55–1.45	10.5 (9.9, 11,0)	0.178	0.660

abilities within each range. We use 500 training points for the Gaussian process emulator (800 for the 10–20% PHENIX bin). We check that the results of the Gaussian emulator are within a few percent of the true blast-wave result. Finally a Markov Chain Monte Carlo provides a likelihood analysis and gives the maximum likelihood parameters and uncertainties.

As discussed above, for the analysis here we will set $\lambda = 2$. We will further restrict the set of simultaneously fitted parameters to seven, choosing $\mathcal{P} = (\tau_{\rm fo}, T_{\rm fo}, R_y/R_x, n, \alpha_0, \alpha_2, \eta/s)$ from the full set $\tilde{\mathcal{P}}$. Two considerations guide our choice to restrict the number of parameters. Some of the parameters we have removed are highly correlated with remaining ones. Sometimes the correlation can be more easily resolved by additional theoretical considerations. For example, our chosen observables depend on R_x, R_y, and $\tau_{\rm fo}$ primarily through the ratio R_y/R_x, which is a main driver for elliptic flow, and through the overall volume $\sim R_x R_y \tau_{\rm fo}$ which determines the normalization of spectra. Dependences on the individual size parameters are absent in the ideal blast wave, but enter in a subleading way through the viscous correction terms. We constrain R_x, R_y, and $T_{\rm fo}$ by fitting the ratio R_y/R_x, and the time $\tau_{\rm fo}$ and by adding in addition the simple geometric estimate

$$R_x \approx (R_0 - b/2) + \tau_{\rm fo} c_\tau (\alpha_0 + \alpha_2), \tag{15}$$

for the propagation of the fireball boundary in the x direction. Here the radius of the colliding nucleus is R_0, and the impact parameter is denoted as b. The expansion parameter $c_\tau = \bar{\alpha}_0/\alpha_0$ relates the *time-averaged* surface velocity $\bar{\alpha}_0$ with its final value α_0 at freeze-out. The boundary velocity parameters α_0 and α_2 at freeze-out are fitted to data. c_τ can be estimated to be between 0.6 and 0.8 going from the most peripheral bin to the most central bin in the analysis. This can be inferred from typical radial velocity-vs-time curves obtained in fluid dynamic simulations [56]. As this is a simple model we vary c_τ in the next section to explore the uncertainties from this choice of parameter reduction. The impact parameter b used for each centrality bin is taken from Glauber Monte Carlo simulations used by the corresponding experiment [53,57].

The speed of sound squared c_s^2 for a hadronic gas is discussed, e.g., in [58,59]. We use [58] to adjust c_s^2 iteratively with the temperature found for each fitted centrality and collision system. The values we find are given in Table I for quick reference. Further below we will explore the dependence of the extracted shear viscosity and temperature on our choice of speed of sound by varying c_s^2. The relevant chemical potentials are not quite settled in the literature. We find good fits for chemical potentials for pions roughly consistent with [58,60]. The values for (μ_π, μ_K, μ_p) for each data set are summarized in Table II. Again we account for the uncertainties by varying the chose values in the uncertainty analysis in the next section.

Error bars for experimental data are crucial input for the statistical analysis. In absence of further details about correlations between error bars we use the statistical and systematic errors quoted by experiments, summed in quadrature, for each momentum bin. This is the main uncertainty input to the MADAI analysis. This procedure works well for ALICE data. Systematic errors for PHENIX-identified hadron P_T spectra are discussed in [50] but numbers are not included in the published data files. We thus start with the provided statistical errors and scale them up. Interestingly, the statistical analysis itself also suggests that statistical error bars alone

TABLE II. Chemical potentials for pion, kaon, and proton for each ALICE and PHENIX data set in its regular fit range, together with the extracted freeze-out temperatures.

Centrality	μ_π (MeV)	μ_K (MeV)	μ_p (MeV)	T (MeV)
		ALICE 2.76 TeV		
10–20%	70	100	245	113
20–30%	64	85	220	118
30–40%	61	73	203	121
40–50%	58	63	190	126
50–60%	55	47	170	130
		PHENIX 0.2 TeV		
10–20%	65	62	200	121
20–40%	61	51	188	124
40–60%	53	22	138	134

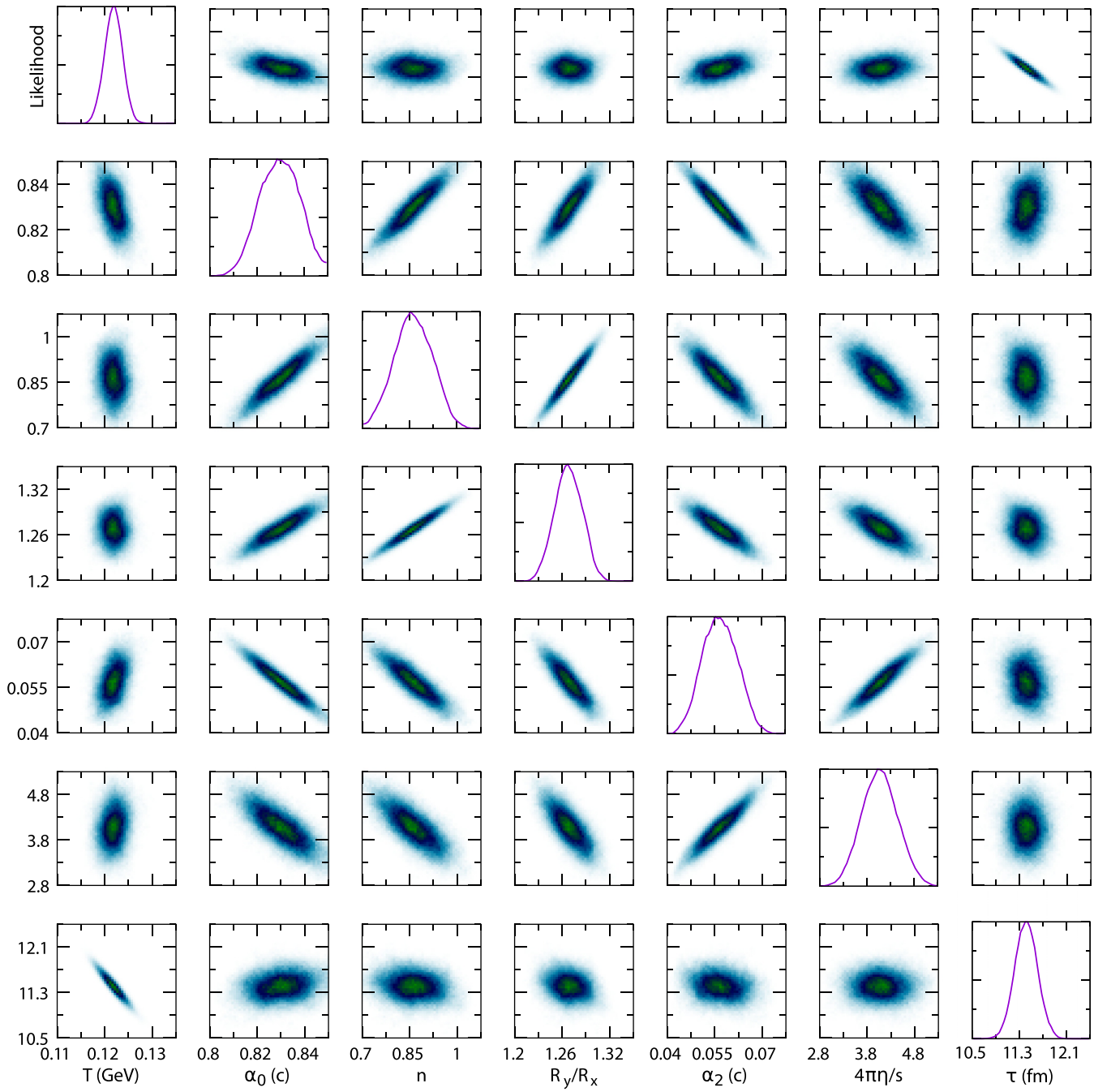

FIG. 1. Likelihood analysis for ALICE data in the 30–40% centrality bin provided by the MADAI package. The horizontal and vertical axes show the chosen prior ranges for the parameters $\mathcal{P}$. From left to right (bottom to top): T (GeV), α_0, n, R_y/R_x, α_2, η/s, τ (fm/c). Plots on the diagonal show posterior likelihood distributions. The off-diagonal plots show correlations between parameters.

for the PHENIX P_T spectra are insufficient in the presence of much larger uncertainties for elliptic flow. This comes about because there is a competition between fits to P_T spectra and v_2 regarding the best value of η/s. Momentum spectra prefer small viscous corrections, while v_2 data typically prefer large viscous corrections. The optimized η/s will be a balance between these constraints. If error bars are unbalanced between spectra and v_2 we see large likelihoods but nevertheless ill-fitting approximations for the quantity with larger error bars. We have to assume that the extraction of η/s is then biased in one direction. It is suggestive to accept an overall larger uncertainty for possibly less bias in the analysis. As a result of these considerations we multiply the statistical error given for PHENIX spectra by factors of 1.5, 3, and 4 for the 10–20%, 20–40%, and 40–60% centrality bins, respectively. Similar considerations apply for the fit to fluid dynamic simulations discussed below. Table III shows the typical relative error in some data sets in the regular fit range (RFR), before adjustments are made. The typical value is defined as the median value within the RFR for all three hadron species.

TABLE III. Typical error percentage, defined as the median for all bins in the RFR, for PHENIX data. The statistical error only is shown for the spectra. For comparison we also show one centrality bin of ALICE data. When two values for the error on v_2 are given they refer to the values in the smaller 10%-wide centrality bins covered.

Total error	PHENIX			ALICE
	10–20%	20–40%	40–60%	30–40%
Spectra (%)	1.23	0.89	0.92	5.65
v_2 (%)	6.71	3.13, 3.29	3.27, 3.80	3.24

IV. FIT RESULTS AND UNCERTAINTY ANALYSIS

With the preparations from the previous sections in place we go ahead and analyze the available data for each energy and centrality bin. The fit results are generally of good quality despite the relatively large RFR fit range. As an example we discuss here the 30–40% centrality bin for ALICE data in detail. Figure 1 shows the results for the fit parameter set $\mathcal{P}$ from the statistical analysis for fits in the RFR of this data set. The likelihood plots on the diagonal of Fig. 1 show well defined peaks. The off-diagonal plots show correlations between fit parameters. The preferred (average) values for this ALICE centrality bin are $\tau_{\rm fo} = 11.41$ fm/c, $T_{\rm fo} = 121.9$ MeV, $\alpha_0 = 0.830c$, $n = 0.87$, $R_y/R_x = 1.270$, $\alpha_2 = 0.0564c$, $\eta/s = 4.06/(4\pi)$. Recall that the values for the external parameters c_τ and c_s^2 as well as for the chemical potentials, and the regular fit range used, are given in Tables I and II, respectively.

Although we have already eliminated some parameters from the blast wave, there are still correlations between the remaining parameters in $\mathcal{P}$. Most prominently there is an expected anti-correlation between freeze-out time and temperature which comes from the constraint on the overall number of particles. Surprisingly there is no pronounced anti-correlation between temperature and radial flow parameter α_0, which means that the choice of three different hadrons to fit, and the sizes of the fit ranges, are sufficient to cleanly separate thermal and collective motion. We note a correlation between the elliptic flow parameter α_2 and η/s. As expected, for larger values of P_T these two parameters move the elliptic flow in different directions, i.e., an increase in one of these parameters will necessitate an increase in the other one. The correlations seen in this centrality bin are found to be qualitatively true for the other energies and centrality bins as well.

Using the preferred parameters, we calculate the transverse momentum spectra and elliptic flow v_2 for the 30–40% ALICE centrality bin. We show these calculations together with the data in Fig. 2. The bottom of the figure shows the ratio of calculation over data. For the majority of P_T bins the deviation is less than 5%, and it rarely exceeds 20%. If the experimental error bars are included, the ratio is consistent with 1 almost everywhere in the RFR.

Next we plot some components of the shear stress tensor $\pi^{\mu\nu}$ found from the fit for this centrality bin. Figure 3 shows the dimensionless ratio $\pi^{\mu\nu}/(e+p)$ for the shear correction to the energy density ($\mu\nu = 00$), the flow in x direction (01), and the flow in y direction (02) as functions of the radius coordinate r for fixed azimuthal angle ϕ (either $\phi = 0$ or $\phi = \pi/2$). We also show $\pi^{\mu\nu}/(e+p)$ for $\mu\nu = 12$ and 22 as a function of ϕ in the first quadrant for two values of the reduced radius ρ. We find that shear stress usually rises towards the outside of the fireball (larger r or ρ). This is consistent with naive expectations for real collision systems where gradients rise away from the center. It is ensured in the blast-wave model

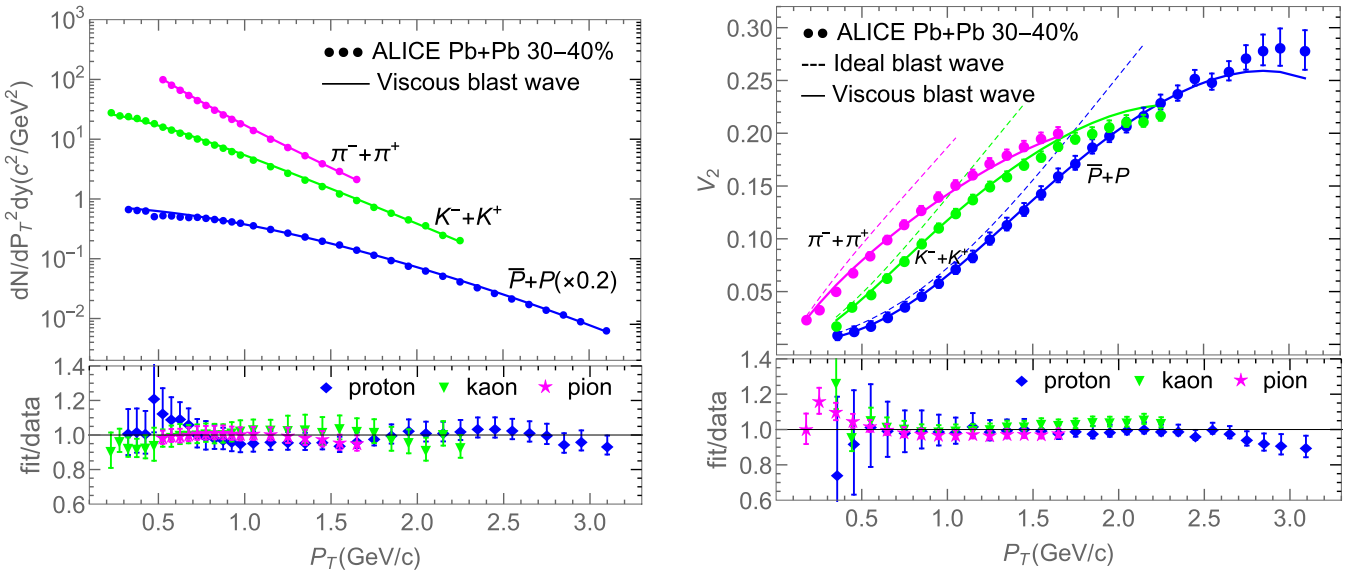

FIG. 2. Left panel: Transverse momentum spectra for pions, kaons, and protons (solid lines), respectively, using the extracted, preferred fit parameters for the ALICE 30–40% centrality bin. We also show the ALICE data used for the fit (circles) with statistical and systematic errors summed in quadrature. Right panel: Elliptic flow v_2 for pions, kaons, and protons (solid lines) for the same parameters, together with ALICE data (circles). We also show the elliptic flow calculated in the ideal case, i.e., without the shear stress term δf in the particle distribution (dashed lines). Ratios of calculations to data are shown below the panels.

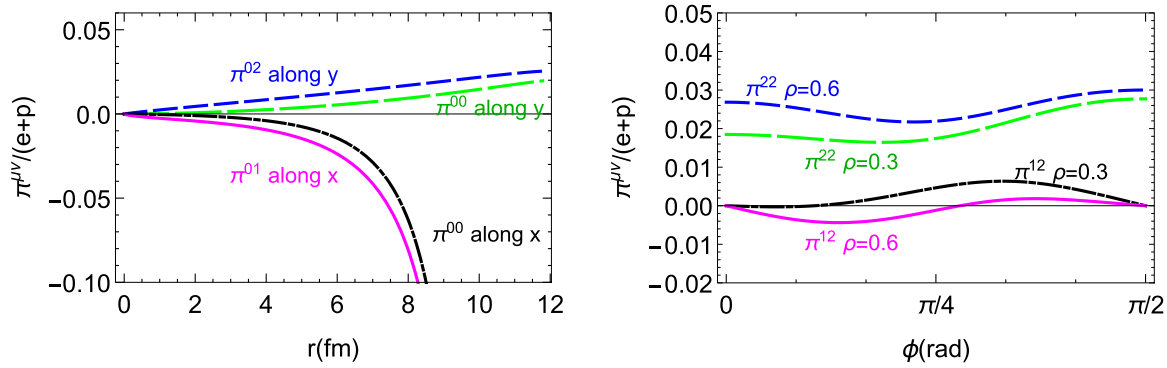

FIG. 3. The dimensionless ratio $\pi^{\mu\nu}/(e+p)$ at midrapidity $\eta_s = 0$ for the blast wave fitted to ALICE 30–40% centrality data. Left panel: π^{00} as a function of radial coordinate r taken along both the positive x axis and the positive y axis. The shear corrections to energy flow in the x direction, π^{01}, is also shown along the positive x axis, and π^{02} is shown along the positive y axis. (Note that the fireball has different sizes in x and y directions.) Right panel: π^{12} and π^{22} as functions of azimuthal angle ϕ in the first quadrant for two values of the dimensionless radius ρ.

by the increasing gradient of the flow four-velocity with ρ. In all situations we find $\pi^{\mu\nu} \lesssim e + p$, and usually the shear stress is significantly smaller than $e + p$. However, this ratio can be somewhat misleading as $e + p$ characterizes a quantity in the rest frame of a fluid cell while $\pi^{\mu\nu}$ is explicitly computed in the laboratory frame.

For an even more enlightening characterization of the effects of shear stress we can compare the ideal energy momentum tensor in the laboratory frame $T^{\mu\nu}_{\rm ideal} = (e + p)u^\mu u^\nu - pg^{\mu\nu}$, scaled by $e + p$, to the full energy momentum tensor $T^{\mu\nu} = T^{\mu\nu}_{\rm ideal} + \pi^{\mu\nu}$ scaled by the same quantity. The difference between both quantities characterizes the size of the viscous correction. In Fig. 4 we show the full and ideal scaled flows in the x direction $[T^{01}/(e + p)$ and $T^{01}_{\rm ideal}/(e + p)]$, as functions of the radial coordinate r along the x direction, as well as the scaled flows in the y direction $[T^{02}/(e + p)$ and $T^{02}_{\rm ideal}/(e + p)]$ as functions of r along the y direction. The comparison of flows in x and y directions is a direct measure of the azimuthal asymmetry in the system. We observe that the maximum correction due to viscous effects, right at the boundary of the fireball, reaches about 30% of $T_{\rm ideal}$, but it is much smaller away from the boundary. The flow along the x direction is larger, as expected from azimuthal asymmetry. We find that the larger x flow is reduced by viscous effects, while the smaller y flow in the y direction is enhanced. Thus, the viscous corrections overall lead to a decrease the observable elliptic flow v_2. This is consistent with expectations and is thus modeled correctly by the viscous blast wave. We can also be cautiously optimistic that viscous corrections are typically small enough to not contradict the use of the Navier-Stokes approximation.

We analyze other centrality bins of ALICE analogous to the 30–40% centrality bin. The results for all ALICE centrality bins are summarized in Table IV. We note that the general trends of parameters as functions of centrality are consistent with expectations. The freeze-out temperature $T_{\rm fo}$ rises toward smaller systems. The boundary velocity α_0 reduces slightly at the same time. The (spatially) averaged radial velocity (not

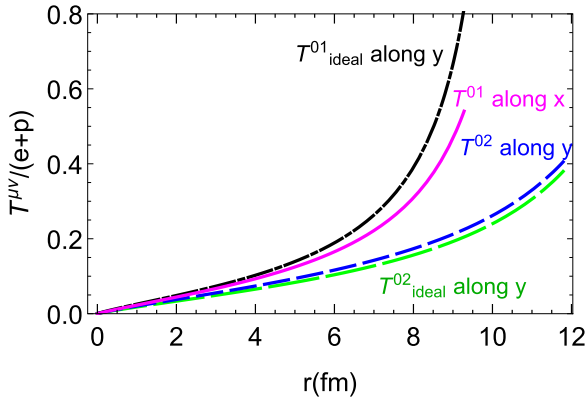

FIG. 4. The dimensionless ratios $T^{0i}_{\rm ideal}/(e + p)$ and $T^{0i}/(e + p)$ at midrapidity $\eta_s = 0$ for the blast wave fitted to ALICE 30–40% centrality data. These quantities are related to the flow in the x direction ($i = 1$) and y direction ($i = 2$). The flow for $i = 1$ is shown along the positive x axis as a function of radial position r and the flow for $i = 2$ is shown along the positive y axis.

TABLE IV. Preferred values for the parameter set $\mathcal{P}$ obtained for different centrality bins for ALICE and PHENIX data in the regular fit range.

Centrality	τ (fm/c)	T (MeV)	α_0/c	n	R_y/R_x	α_2/c	$4\pi\eta/s$
			ALICE 2.76 TeV				
10–20%	14.76	113.3	0.856	0.78	1.143	0.0355	5.89
20–30%	13.05	118.0	0.839	0.80	1.200	0.0517	5.45
30–40%	11.41	121.9	0.830	0.87	1.270	0.0564	4.06
40–50%	9.96	125.5	0.835	1.07	1.362	0.0472	2.46
50–60%	8.72	130.1	0.823	1.27	1.433	0.0427	1.66
			PHENIX 0.2 TeV				
10–20%	10.9	121.2	0.734	0.80	1.090	0.0463	3.32
20–30%	9.28	123.5	0.742	0.94	1.167	0.0528	1.98
30–40%	9.08	124.2	0.733	0.90	1.227	0.0576	1.64
40–50%	7.15	132.2	0.704	1.03	1.312	0.0631	1.08
50–60%	6.96	135.3	0.689	1.00	1.354	0.0630	0.93

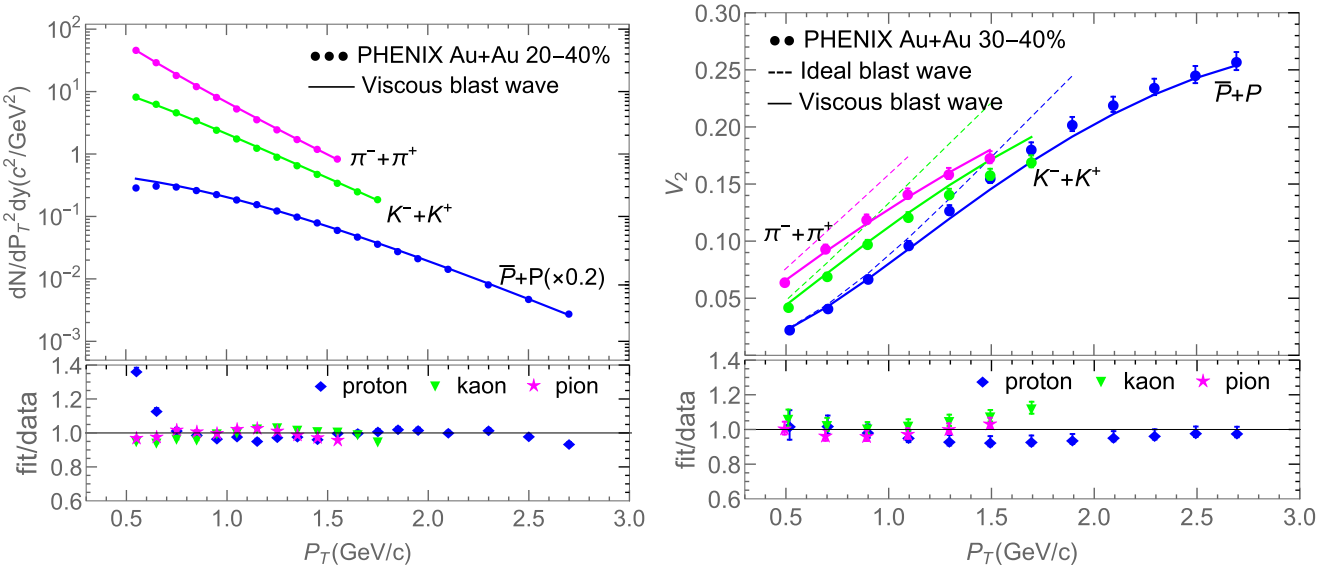

FIG. 5. Same as Fig. 2 for the PHENIX 30–40% centrality bin (20–40% for the spectrum). Statistical errors only are shown for PHENIX spectra.

shown) drops more significantly due to the concurrent change in the radial shape parameter n. These systematic trends give an important qualitative check of the fit results. However, we will not be interested in further interpretation of fit parameters other than the temperature and specific shear viscosity. The ALICE data sets provide us with a range of temperatures from roughly 113 to 130 MeV.

Generally, the azimuthal flow deformation parameter α_2 and spatial deformation R_y/R_x as well as the specific shear viscosity η/s are most sensitive to the elliptic flow data. We indicate the sensitivity of the calculated elliptic flow on η/s at freeze-out by also showing in Fig. 2 the elliptic flow computed with the same parameters but without the correction term δf. As expected, at large P_T the corrections from δf are largest, thus extracted values of η/s are very sensitive to v_2 at large P_T. Note, however. that despite the p^2 dependence of δf in the local rest frame, the correction to v_2 due to δf does not have to strictly vanish at small transverse momenta P_T in the *laboratory frame*. We have to be mindful that δf can not be too large. As discussed earlier, higher order corrections in shear stress would have to be taken into account if $\delta f \approx f$. We have chosen the RFR such that v_2 starts to deviate from the equilibrium behavior at large P_T, but we generally exclude points for which the slope of v_2 turns negative. In the RFR we find that the viscous correction is largest for protons, topping out at 19% for the largest P_T bin in the spectrum for the 40–50% centrality bin. For kaons and pions the largest corrections for the spectra we find are 11% and 4%, respectively. The typical size of viscous corrections is much smaller than the maximum numbers quoted here.

We repeat the analysis with data from PHENIX in 200 GeV Au + Au collisions. The preferred, average values are also summarized in Table IV. The fits with preferred parameter values for one centrality bin are shown in Fig. 5 together with PHENIX data. The behavior of parameters as a function of centrality is similar to the one discussed for the ALICE data sets. The extracted temperature range, roughly 122 to 136 MeV, overlaps with ALICE. It is an important consistency check that the extracted values for η/s are consistent between ALICE data taken at $\sqrt{s_{NN}} = 2.76$ TeV and PHENIX data taken at $\sqrt{s_{NN}} = 0.2$ TeV, within uncertainties. We summarize the results for η/s vs temperature T from all data sets in Fig. 6. The main qualitative feature is a decrease in η/s with increasing temperature, as would be expected from general principles. However, values close to the lower bound are already reached at the upper end of the temperature range.

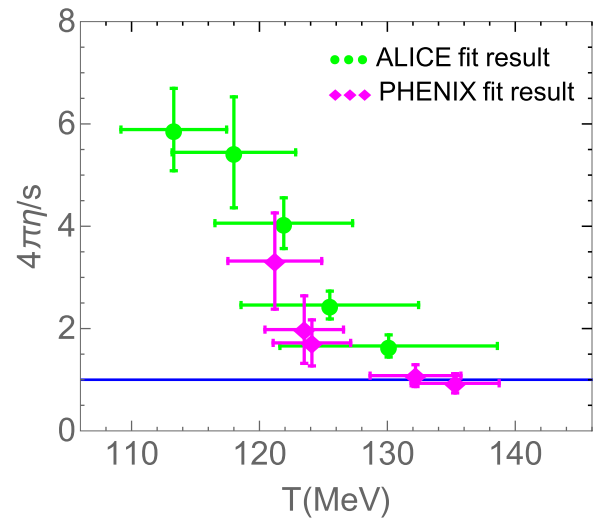

FIG. 6. Specific shear viscosity η/s at corresponding kinetic freeze-out temperature T extracted from the available ALICE and PHENIX centrality bins before removing blast-wave bias. Uncertainties shown are combined uncertainties of types (III) and (IV) explained in the text. Note that the values of the chemical potentials for stable hadrons are nonzero for all of these points.

TABLE V. Definitions of different fit ranges for ALICE spectrum data in the 30–40% centrality bin. The ranges for v_2 data are chosen commensurately. Also shown are the extracted temperature and specific shear viscosity for each fit range.

Fit range (GeV/c)	Proton	Kaon	Pion	T (MeV)	$4\pi\eta/s$
Low (LFR)	0.325–2.05	0.225–1.25	0.19–0.825	113.4	3.85
Regular (RFR)	0.325–3.1	0.225–2.25	0.525–1.65	121.9	4.06
High (HFR)	1.25–3.1	0.725–2.25	0.825–1.65	125.2	3.43

Let us now turn to a discussion of the uncertainties in our analysis. We can group them into four categories, ranging from basic statistical errors to those rather fundamental in nature: (I) Limitations in the freeze-out ansatz that are shared between blast wave and fluid dynamics, in particular the assumption of a sharp freeze-out hypersurface for all particle species. (II) Uncertainties and biases from assumptions made in our blast-wave model compared to fluid dynamics, e.g. the simple ansatz for the freeze-out hypersurface and the flow field, the lack of resonance decays and bulk stress effects, and the Navier-Stokes approximation for shear stress. (III) Uncertainties from our choice of external parameters and choice of fit ranges. (IV) Uncertainties from the errors in experimental data and the quality of the Gaussian emulator. A thorough analysis of item (I) is beyond the scope of this paper and can not be achieved within the blast-wave model or fluid dynamics. However we will analyze the other three sources of uncertainty.

Uncertainties in extracted parameters from the error bars in our data sets and statistical analysis [type (IV)], are provided by the MADAI code. We quote the widths σ_T^{stat}, $\sigma_\eta^{\text{stat}}$ of temperature and specific shear viscosity for each centrality bin and energy. We estimate uncertainties summarized under (III) by systematically varying the underlying assumptions. For example, as discussed earlier we choose alternative fit ranges which are shifted to lower (LFR) or larger (HFR) P_T. Limitations apply as we do not want to push too far into regions where we expect our blast wave to fail; see the discussion of fit ranges in Sec. III. We discuss results once more for the 30–40% ALICE centrality bin as an example. For the uncertainty analysis we focus on the results for the extracted temperature and specific shear viscosity. Table V shows the three fit ranges, LFR, RFR, HFR, for all three particle species for this data set. Both temperature and η/s show moderate dependencies on the fit range. This is expected for the temperature, where a change in P_T samples different admixtures of resonance decays in spectra with different slopes and thus apparent temperatures. We parametrize the deviations seen from the RFR values as Gaussian distributions with widths σ_k^{range} $(k = T, \eta)$. We repeat this analysis for all other centralities and energies with qualitatively similar results.

As discussed earlier we also study the effects of variations in the chemical potential, speed of sound squared, and the expansion parameter c_τ. Table VI shows the values for T and η/s extracted for the 30–40% ALICE centrality bin for ± 15 MeV variations in the pion chemical potential. We find that the temperature is rather insensitive to variations of μ_π while η/s displays moderate sensitivity. We again assign Gaussian widths σ_k^μ $(k = T, \eta)$ for the uncertainty from this source. We proceed similarly with variations in c_s^2, see Table VII, and c_τ (Table VIII). In both cases we find again very little influence on the extracted temperature. We combine the uncertainties of types (III) and (IV) by adding the individual widths σ_T^i and σ_η^i in quadrature. Note that this assumption of Gaussian behavior here is simply an approximation. The error bars in T and η/s shown in Fig. 6 are the result of this analysis. Table IX summarizes the uncertainties for the ALICE 30–40% centrality bin.

Finally we deal with uncertainties of type (II). Our blast wave is systematically compared to viscous fluid dynamics in detail in an accompanying publication [44]. We briefly summarize the results relevant for this work. In order to quantify what happens to parameters in fluid dynamics when their complex final states are fitted by blast waves, we apply the same blast-wave analysis carried out here to particle spectra and elliptic flow generated with the viscous fluid dynamic code MUSIC [47]. The key point is that in the case of MUSIC the temperature of freeze-out and the specific shear viscosity are set in the code as $(T, \eta/s)_{\text{true}}$ and can be compared to the raw fitted values $(T, \eta/s)_{\text{fit}}$. Let us recall that there are five main simplifications compared to fluid dynamics in our blast wave: (a) simplified hypersurface, (b) simplified flow field, (c) absence of resonance production and decay, (d) absence of bulk stress corrections to particle distributions, and (e) Navier-Stokes approximation to shear stress. While Ref. [44] focuses on the compound effect, one could in principle study the effect of each of these simplifications separately. The first takeaway message of Ref. [44] is that blast-wave fits reproduce the true specific shear viscosities within expected uncertainties. Fitted

TABLE VI. The freeze-out temperature T and specific shear viscosity η/s extracted for different values of pion chemical potential μ_π as explained in the text, for the ALICE 30–40% centrality bin.

	μ_π (MeV)	T (MeV)	$4\pi\eta/s$
less	46	121.0	4.01
regular	61	121.9	4.06
more	76	122.7	3.85

TABLE VII. The same as Table VI for a variation of the speed of sound squared c_s^2 for the ALICE 30–40% centrality bin.

	$c_s^2(c^2)$	T (MeV)	$4\pi\eta/s$
small	0.15	121.8	4.27
regular	0.166	121.9	4.06
large	0.182	122.0	3.85

TABLE VIII. The same as Table VI for a variation of time-averaged surface velocity parameter c_τ for the ALICE 30–40% centrality bin.

	c_τ	T (MeV)	$4\pi\eta/s$
small	0.666	121.6	3.82
regular	0.720	121.9	4.06
large	0.781	121.2	4.12

TABLE IX. A summary of uncertainties σ_T^i and σ_η^i for temperature and specific shear viscosity, respectively, for the 30–40% ALICE centrality bin. Here i refers to the different contributions discussed in the text.

Origin of uncertainty	Stat. analysis	Fit range	μ_π	c_s^2	c_τ	Total σ
T (MeV)	1.90	4.97	0.69	0.08	0.29	5.38
$4\pi\eta/s$	0.35	0.26	0.10	0.17	0.13	0.50

freeze-out temperatures are good for more central collisions, but fall below the true values in peripheral collisions. Overall our viscous blast wave turns out to be a very useful estimator.

As a second step in [44] a map $M : (T, \eta/s)_{\text{true}} \to (T, \eta/s)_{\text{fit}}$ is created from an array of parameter values, and approximated by a linear fit. This was done for both Pb + Pb collisions at LHC energies and Au + Au collisions at RHIC energies. Uncertainties of these maps M have also been estimated in Ref. [44]. By inverting M from Ref. [44] we can correct the raw fit results $(T, \eta/s)_{\text{fit}}$ obtained here from experimental data. This will remove the bias introduced by the blast-wave approximations (a)–(e) compared to what a full fluid dynamic fit could achieve. What remain are uncertainties of type (I) from which fluid dynamics suffers as well. The correction step $(T, \eta/s)_{\text{fit}} \to (T, \eta/s)_{\text{corrected}}$ applied to our fits of experimental data leaves the results for smaller temperatures unchanged within uncertainties but leads to a slower drop of η/s at larger temperatures compared to the raw fit result in Fig. 6. We also propagate the error estimated for the raw results through M^{-1} and add the uncertainty from the determination of M itself [44]. The final corrected result with compounded uncertainties is shown in Fig. 8.

V. DISCUSSION

We have introduced a blast-wave model with viscous corrections due to shear stress in the Navier-Stokes approximation. The blast-wave model can obtain excellent fits to hadron spectra and v_2 over a large range of P_T. The viscous correction term helps to describe the slow down of the growth of v_2 with P_T. This model provides a reliable instrument that can give useful snapshots of the dynamically evolving fireball.

To further demonstrate the usefulness we plot predictions for the spectra and v_2 for two more particles, the Λ baryon and the deuteron d, in a mid-central bin as examples. The results are shown in Fig. 7 together with ALICE data [49,61,62]. Note that our calculation is a prediction in the sense that Λ and deuteron data have not been used to fix the blast-wave parameters. Chemical potentials for both species have been fixed to 344 and 314 MeV respectively. We find overall good agreement for this centrality bin. This is interesting since there have been questions in both cases about the validity of a common freeze-out with stable hadrons. In particular the deuteron is often thought to be emerging from coalescence processes after freeze-out [61,63,64]. We find that, whatever the detailed mechanism of deuteron creation, the spectra and elliptic flow are described reasonably well by the same

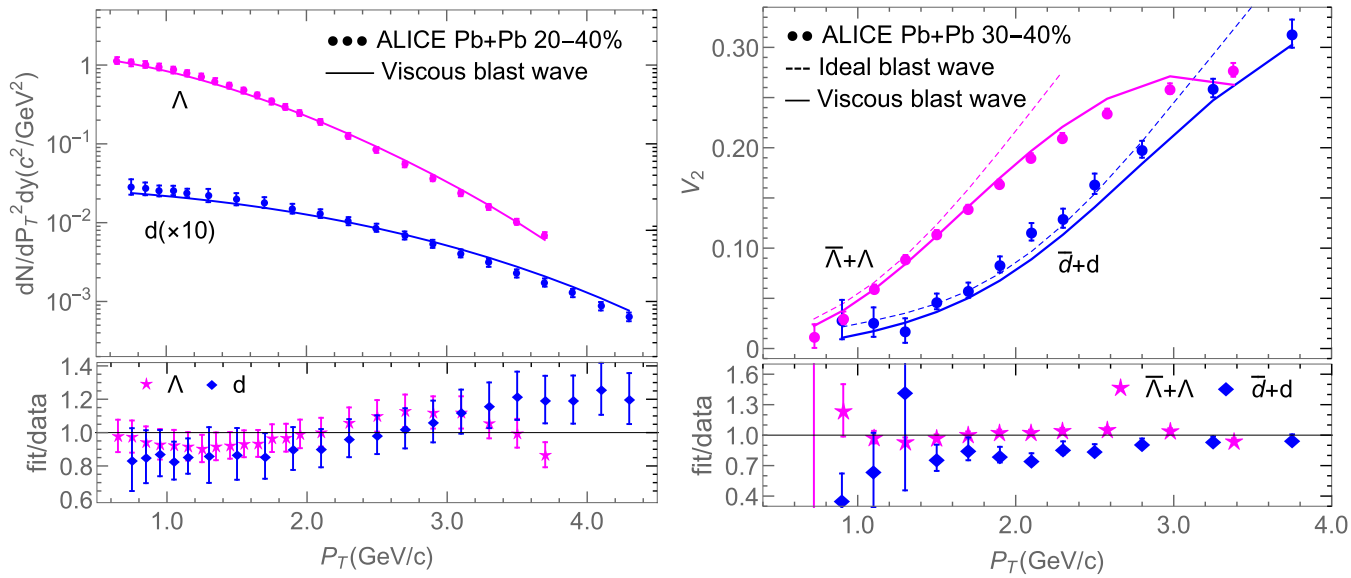

FIG. 7. Left panel: Transverse momentum spectra for Λ's and deuterons (solid lines), respectively, calculated for the 20–40% centrality bin in Pb + Pb collisions together with ALICE data (symbols). Right panel: Elliptic flow v_2 for $\Lambda + \bar{\Lambda}$ and $d + \bar{d}$ (solid lines) in the 30–40% centrality bin together with ALICE data (circles). We again show the elliptic flow calculated in the ideal case as well. In both cases the preferred parameters for the 30–40% centrality bin extracted for stable charged hadrons has been used.

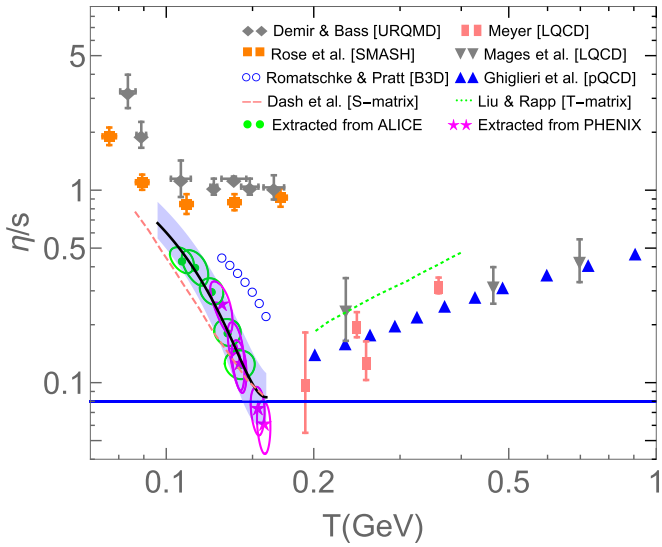

FIG. 8. The results of this paper, corrected for blast-wave bias, compared to various calculations of the specific shear viscosity η/s as a function of temperature. A line and uncertainty band have been drawn through our points to guide the eye. Details are in the text.

temperature and flow field that also describes stable hadrons, at least in mid-central collisions.

Let us now turn to a discussion of the particular application of our blast wave we have focused on here. From two different collision systems, Pb + Pb at LHC energy and Au + Au at top RHIC energy, we have extracted the blast-wave parameters, including freeze-out temperatures, η/s, and parameters describing the collective flow field at freeze-out. We find that the viscous shear tensor that can be reconstructed from the fits behaves qualitatively as expected, which serves as a sanity check on the viscous corrections implemented for the blast wave. For example, we find a reduction in the azimuthal flow asymmetry due to viscous corrections. The correction to equilibrium values of the stress energy tensor are typically small enough to justify our assumptions *a posteriori*.

By analyzing several centralities at LHC and RHIC we obtain a set of η/s-vs-T points that are consistent with each other within estimated uncertainties. They give a first (uncorrected) temperature dependence of η/s between roughly 110 to 140 MeV, reaching the proposed lower bound at the latter temperature. We have carefully analyzed uncertainties of the fit results. In particular, we have studied uncertainties of type (II) that arise from the simplifying assumptions made in blast-wave models compared to fluid dynamics. Using Ref. [44] we find a systematic bias that slightly underestimates the temperature T at larger temperatures. When we correct for this bias we arrive at the final result shown by the dots and stars in Fig. 8 with the compound uncertainties shown as ellipses. In the same figure we show results for the hadronic phase η/s from hadronic cascades URQMD [21], B3D [23], and SMASH [24]. They generally show larger values of η/s above $T \approx 100$ MeV, but one could speculate that below $T \approx 100$ MeV the results might converge within uncertainties, as the URQMD and SMASH results switch their behavior to a temperature slope similar to our results. Unfortunately we do not have the data points to confirm this. Interestingly, a more recent calculation by Dash *et al.* [25] traces our result nicely within uncertainties. We also show several calculations of the specific shear viscosity in the QGP phase, from lattice QCD [30–32], T-matrix calculations [65], and next-to-leading perturbative QCD [37].

After correcting the bias our extracted η/s reaches the proposed lower bound around the pseudocritical temperature T_c. Overall these results together are consistent with the idea of a minimum of the specific shear viscosity around T_c. Our result specifically would indicate that interactions in the hadronic phase continue to be strong just below T_c while several hadronic transport suggests a more abrupt change below T_c. The grey band in Fig. 8 represents a simple parametrization of our result. The center line is $\eta/s = 1.46 \times 10^2 \times (0.160 - T)^2 + 0.08$, where T is measured in GeV. This is the preferred value of η/s as a function of T between 100 and 160 MeV temperature. We need to keep in mind that relatively large chemical potentials for stable hadrons build up in the collision systems that we have analyzed here. For example, the chemical potential for pions is as large as 70 MeV at the lowest temperature points we have extracted. Thus Fig. 8 is a projection of a more complicated plot with additional chemical potential axes. Studies have indicated that finite chemical potentials can indeed lead to smaller values of η/s in hadronic transport models [21].

The fate of η/s in the hadronic phase continues to be intriguing. We have added a scenario, based on extraction from data, that predicts a steady rise of η/s while the temperature drops from around T_c to 110 MeV, and chemical potentials increase. Our approach is rooted in data taken in heavy ion collisions but has a long list of uncertainties. We have quantified the more accessible uncertainties (IV), (III) related to the analysis itself and to systemic uncertainties from choices made during the analysis. We have also made an attempt to estimate and remove the bias of blast-wave fits compared to full fluid dynamic simulations [type (II)]. More fundamental uncertainties remain which may be quantified elsewhere. In particular, there is the question of how the extracted values for η/s connect to the mean-free path of the system which increases rapidly during freeze-out. Certain aspects of the current analysis will be improved in the near term future. For example the detailed energy dependence of the shear stress term, parametrized by λ, and the effects of bulk stress could be included, albeit at the expense of adding two parameters to the analysis. One could also include an analysis of the asymmetry coefficient v_4, which requires a generalization of both hypersurface and flow field of the blast wave. Lastly, resonances and their decays could in principle be included in the calculation.

ACKNOWLEDGMENTS

Z.Y. would like to thank Yifeng Sun and Shuai Y. F. Liu for useful discussions. R.J.F. would like to thank Charles Gale and Sangyong Jeon for comments and their hospitality at McGill University where part of this work was carried out. R.J.F. also acknowledges useful discussions with Amaresh Jaiswal and Ron Belmont. We thank Che-Ming Ko, Jürgen

Schukraft, and Ulrich Heinz for valuable comments. This work was supported by the U.S. National Science Foundation under Awards No. 1516590, No. 1550221, and No. 1812431.

[1] J. C. Collins and M. J. Perry, Superdense Matter: Neutrons or Asymptotically Free Quarks?, Phys. Rev. Lett. **34**, 1353 (1975).
[2] E. V. Shuryak, Quark-gluon plasma and hadronic production of leptons, photons and psions, Phys. Lett. B **78**, 150 (1978).
[3] M. Gyulassy and L. McLerran, New forms of QCD matter discovered at RHIC, Nucl. Phys. A **750**, 30 (2005).
[4] E. Shuryak, Physics of strongly coupled quark-gluon plasma, Prog. Part. Nucl. Phys. **62**, 48 (2009).
[5] P. F. Kolb, P. Huovinen, U. W. Heinz, and H. Heiselberg, Elliptic flow at SPS and RHIC: From kinetic transport to hydrodynamics, Phys. Lett. B **500**, 232 (2001).
[6] P. Huovinen, P. F. Kolb, U. W. Heinz, P. V. Ruuskanen, and S. A. Voloshin, Radial and elliptic flow at RHIC: Further predictions, Phys. Lett. B **503**, 58 (2001).
[7] P. Romatschke and U. Romatschke, Viscosity Information from Relativistic Nuclear Collisions: How Perfect is the Fluid Observed at RHIC?, Phys. Rev. Lett. **99**, 172301 (2007).
[8] K. Dusling and D. Teaney, Simulating elliptic flow with viscous hydrodynamics, Phys. Rev. C **77**, 034905 (2008).
[9] B. Schenke, S. Jeon, and C. Gale, Anisotropic flow in $\sqrt{s} =$ 2.76 TeV Pb+Pb collisions at the LHC, Phys. Lett. B **702**, 59 (2011).
[10] U. Heinz and R. Snellings, Collective flow and viscosity in relativistic heavy-ion collisions, Annu. Rev. Nucl. Part. Sci. **63**, 123 (2013).
[11] P. K. Kovtun, D. T. Son, and A. O. Starinets, Viscosity in Strongly Interacting Quantum Field Theories from Black Hole Physics, Phys. Rev. Lett. **94**, 111601 (2005).
[12] D. Teaney, The Effects of viscosity on spectra, elliptic flow, and HBT radii, Phys. Rev. C **68**, 034913 (2003).
[13] H. Song, S. A. Bass, and U. Heinz, Viscous QCD matter in a hybrid hydrodynamic+Boltzmann approach, Phys. Rev. C **83**, 024912 (2011).
[14] H. Song, S. A. Bass, U. Heinz, T. Hirano, and C. Shen, Hadron spectra and elliptic flow for 200 A GeV Au+Au collisions from viscous hydrodynamics coupled to a Boltzmann cascade, Phys. Rev. C **83**, 054910 (2011); **86**, 059903(E) (2012).
[15] M. Prakash, M. Prakash, R. Venugopalan, and G. Welke, Nonequilibrium properties of hadronic mixtures, Phys. Rep. **227**, 321 (1993).
[16] S. Muroya and N. Sasaki, A Calculation of the viscosity over entropy ratio of a hadronic gas, Prog. Theor. Phys. **113**, 457 (2005).
[17] A. Dobado and F. J. Llanes-Estrada, The Viscosity of meson matter, Phys. Rev. D **69**, 116004 (2004).
[18] J. W. Chen and E. Nakano, Shear viscosity to entropy density ratio of QCD below the deconfinement temperature, Phys. Lett. B **647**, 371 (2007).
[19] K. Itakura, O. Morimatsu, and H. Otomo, Shear viscosity of a hadronic gas mixture, Phys. Rev. D **77**, 014014 (2008).
[20] A. Dobado, F. J. Llanes-Estrada, and J. M. Torres-Rincon, η/s and phase transitions, Phys. Rev. D **79**, 014002 (2009).
[21] N. Demir and S. A. Bass, Shear-Viscosity to Entropy-Density Ratio of a Relativistic Hadron Gas, Phys. Rev. Lett. **102**, 172302 (2009).
[22] D. Fernandez-Fraile and A. Gomez Nicola, Transport coefficients and resonances for a meson gas in chiral perturbation theory, Eur. Phys. J. C **62**, 37 (2009).
[23] P. Romatschke and S. Pratt, Extracting the shear viscosity of a high temperature hadron gas, arXiv:1409.0010.
[24] J.-B. Rose, J. M. Torres-Rincon, A. Schäfer, D. R. Oliinychenko, and H. Petersen, Shear viscosity of a hadron gas and influence of resonance lifetimes on relaxation time, Phys. Rev. C **97**, 055204 (2018).
[25] A. Dash, S. Samanta, and B. Mohanty, Transport coefficients for multicomponent gas of hadrons using Chapman-Enskog method, Phys. Rev. D **100**, 014025 (2019).
[26] H. Niemi, G. S. Denicol, P. Huovinen, E. Molnar, and D. H. Rischke, Influence of a temperature-dependent shear viscosity on the azimuthal asymmetries of transverse momentum spectra in ultrarelativistic heavy-ion collisions, Phys. Rev. C **86**, 014909 (2012).
[27] J. E. Bernhard, P. W. Marcy, C. E. Coleman-Smith, S. Huzurbazar, R. L. Wolpert, and S. A. Bass, Quantifying properties of hot and dense QCD matter through systematic model-to-data comparison, Phys. Rev. C **91**, 054910 (2015).
[28] C. Gale, S. Jeon, and B. Schenke, Hydrodynamic modeling of heavy-ion collisions, Int. J. Mod. Phys. A **28**, 1340011 (2013).
[29] P. Romatschke and U. Romatschke, *Relativistic Fluid Dynamics In and Out of Equilibrium And Applications to Relativistic Nuclear Collisions*, Cambridge Monographs on Mathematical Physics (Cambridge University Press, Cambridge, 2019).
[30] H. B. Meyer, Calculation of the shear viscosity in SU(3) gluodynamics, Phys. Rev. D **76**, 101701(R) (2007).
[31] H. B. Meyer, Transport properties of the quark-gluon plasma from lattice QCD, Nucl. Phys. A **830**, 641c (2009).
[32] S. W. Mages, S. Borsányi, Z. Fodor, A. Schäfer, and K. Szabó, Shear viscosity from lattice QCD, PoS **LATTICE 2014**, 232 (2015).
[33] M. Haas, L. Fister, and J. M. Pawlowski, Gluon spectral functions and transport coefficients in Yang–Mills theory, Phys. Rev. D **90**, 091501(R) (2014).
[34] N. Astrakhantsev, V. Braguta, and A. Kotov, Temperature dependence of shear viscosity of $SU(3)$–gluodynamics within lattice simulation, J. High Energy Phys. 04 (2017) 101.
[35] P. B. Arnold, G. D. Moore, and L. G. Yaffe, Transport coefficients in high temperature gauge theories. 1. Leading log results, J. High Energy Phys. 11 (2000) 001.
[36] P. B. Arnold, G. D. Moore, and L. G. Yaffe, Transport coefficients in high temperature gauge theories. 2. Beyond leading log, J. High Energy Phys. 05 (2003) 051.
[37] J. Ghiglieri, G. D. Moore, and D. Teaney, QCD Shear Viscosity at (almost) NLO, J. High Energy Phys. 03 (2018) 179.
[38] L. P. Csernai, J. I. Kapusta, and L. D. McLerran, Strongly Interacting Low-Viscosity Matter Created in Relativistic Nuclear Collisions, Phys. Rev. Lett. **97**, 152303 (2006).
[39] G. D. Westfall, J. Gosset, P. J. Johansen, A. M. Poskanzer, W. G. Meyer, H. H. Gutbrod, A. Sandoval, and R. Stock, Nuclear Fireball Model for Proton Inclusive Spectra from Relativistic Heavy-Ion Collisions, Phys. Rev. Lett. **37**, 1202 (1976).

[40] E. Schnedermann, J. Sollfrank, and U. W. Heinz, Thermal phenomenology of hadrons from 200*A* GeV S+S collisions, Phys. Rev. C **48**, 2462 (1993).

[41] F. Retiere and M. A. Lisa, Observable implications of geometrical and dynamical aspects of freeze-out in heavy ion collisions, Phys. Rev. C **70**, 044907 (2004).

[42] A. Jaiswal and V. Koch, A viscous blast-wave model for relativistic heavy-ion collisions, arXiv:1508.05878.

[43] M. Damodaran, D. Molnar, G. G. Barnaföldi, D. Berényi, and M. Ferenc Nagy-Egri, Testing and improving shear viscous phase space correction models, arXiv:1707.00793.

[44] Z. Yang and R. J. Fries, Parameterizing smooth viscous fluid dynamics with a viscous blast wave, arXiv:2007.11777.

[45] F. Cooper and G. Frye, Single-particle distribution in the hydrodynamic and statistical thermodynamic models of multiparticle production, Phys. Rev. D **10**, 186 (1974).

[46] B. Schenke, S. Jeon, and C. Gale, (3+1)D hydrodynamic simulation of relativistic heavy-ion collisions, Phys. Rev. C **82**, 014903 (2010).

[47] S. Ryu, J.-F. Paquet, C. Shen, G. S. Denicol, B. Schenke, S. Jeon, and C. Gale, Importance of the Bulk Viscosity of QCD in Ultrarelativistic Heavy-Ion Collisions, Phys. Rev. Lett. **115**, 132301 (2015).

[48] J. Adam *et al.* (ALICE Collaboration), Centrality dependence of the nuclear modification factor of charged pions, kaons, and protons in Pb-Pb collisions at $\sqrt{s_{NN}} = 2.76$ TeV, Phys. Rev. C **93**, 034913 (2016).

[49] B. B. Abelev *et al.* (ALICE Collaboration), Elliptic flow of identified hadrons in Pb-Pb collisions at $\sqrt{s_{\rm NN}} = 2.76$ TeV, J. High Energy Phys. 06 (2015) 190.

[50] A. Adare *et al.* (PHENIX Collaboration), Spectra and ratios of identified particles in Au+Au and $d+$Au collisions at $\sqrt{s_{NN}} = 200$ GeV, Phys. Rev. C **88**, 024906 (2013).

[51] A. Adare *et al.* (PHENIX Collaboration), Measurement of the higher-order anisotropic flow coefficients for identified hadrons in Au + Au collisions at $\sqrt{s_{_{NN}}} = 200$ GeV, Phys. Rev. C **93**, 051902 (2016).

[52] J. Sollfrank, P. Koch, and U. W. Heinz, Is there a low-p_T "anomaly" in the pion momentum spectra from relativistic nuclear collisions?, Z. Phys. C **52**, 593 (1991).

[53] B. Abelev *et al.* (ALICE Collaboration), Centrality dependence of π, K, p production in Pb-Pb collisions at $\sqrt{s_{NN}} = 2.76$ TeV, Phys. Rev. C **88**, 044910 (2013).

[54] MADAI Collaboration, https://madai-public.cs.unc.edu/, accessed June 20, 2016.

[55] J. E. Bernhard, J. S. Moreland, S. A. Bass, J. Liu, and U. Heinz, Applying Bayesian parameter estimation to relativistic heavy-ion collisions, Phys. Rev. C **94**, 024907 (2016).

[56] H. Song and U. W. Heinz, Interplay of shear and bulk viscosity in generating flow in heavy-ion collisions, Phys. Rev. C **81**, 024905 (2010).

[57] S. S. Adler *et al.* (PHENIX Collaboration), Suppressed π^0 Production at Large Transverse Momentum in Central Au + Au Collisions at $\sqrt{s_{NN}} = 200$ GeV, Phys. Rev. Lett. **91**, 072301 (2003).

[58] D. Teaney, Chemical freezeout in heavy ion collisions, Phys. Rev. C **61**, 006409 (2001).

[59] P. Huovinen and P. Petreczky, QCD equation of state and hadron resonance gas, Nucl. Phys. A **837**, 26 (2010).

[60] T. Hirano and K. Tsuda, Ultrarelativistic heavy-ion collisions, in *Proceedings of the 30th International Workshop on Gross Properties of Nuclei and Nuclear Excitations, Hirschegg, Austria, 2002*, edited by M. Buballa, W. Norenberg, B. J. Schaefer, and J. Wambach (GSI, Darmstadt, Germany, 2002), pp. 152–157.

[61] S. Acharya *et al.* (ALICE Collaboration), Measurement of deuteron spectra and elliptic flow in Pb–Pb collisions at $\sqrt{s_{\rm NN}} = 2.76$ TeV at the LHC, Eur. Phys. J. C **77**, 658 (2017).

[62] B. B. Abelev *et al.* (ALICE Collaboration), Multi-strange baryon production at mid-rapidity in Pb-Pb collisions at $\sqrt{s_{NN}} = 2.76$ TeV, Phys. Lett. B **728**, 216 (2014); **734**, 409(E) (2014).

[63] L. Adamczyk *et al.* (STAR Collaboration), Measurement of elliptic flow of light nuclei at $\sqrt{s_{NN}} = 200$, 62.4, 39, 27, 19.6, 11.5, and 7.7 GeV at the BNL Relativistic Heavy Ion Collider, Phys. Rev. C **94**, 034908 (2016).

[64] L. Zhu, H. Zheng, C. M. Ko, and Y. Sun, Light nuclei production in Pb+Pb collisions at $\sqrt{s_{NN}} = 2.76$ TeV, Eur. Phys. J. A **54**, 175 (2018).

[65] S. Y. F. Liu and R. Rapp, Spectral and transport properties of a non-perturbative quark-gluon plasma, Eur. Phys. J. A **56**, 44 (2020).